COLORIZATION TRANSFORMER

Anonymous authors
Paper under double-blind review

ABSTRACT

We present the Colorization Transformer, a novel approach for diverse high fidelity image colorization based on self-attention. Given a grayscale image, the colorization proceeds in three steps. We first use an autoregressive transformer to produce a low resolution coarse coloring of the grayscale image. Our architecture adopts conditional transformer layers to effectively capture grayscale input. Two subsequent fully parallel networks upsample the coarse colored low resolution image into a finely colored high resolution image. Sampling from the Colorization Transformer produces diverse colorings whose fidelity outperforms the previous state-of-the-art on colorising ImageNet based on FID results and based on a human evaluation in a Mechanical Turk test. Remarkably, in more than 60% of cases human evaluators prefer the highest rated among three generated colorings over the ground truth.

1 INTRODUCTION

Figure 1: Samples of our model showing diverse, high-fidelity colorizations.

Image colorization is a challenging, inherently stochastic task that requires a semantic understanding of the scene as well as knowledge of the world. Core immediate applications of the technique include producing organic new colorizations of existing image and video content as well as giving life to originally grayscale media, such as old archival images (Tsaftaris et al., 2014), videos (Geshwind, 1986) and black-and-white cartoons (Sỳkora et al., 2004; Qu et al., 2006; Cinarel & Zhang, 2017). Colorization also has important technical uses as a way to learn meaningful representations without explicit supervision (Zhang et al., 2016; Larsson et al., 2016; Vondrick et al., 2018) or as an unsupervised data augmentation technique, whereby diverse semantics-preserving colorizations of labelled images are produced with a colorization model trained on a potentially much larger set of unlabelled images.

The current state-of-the-art in automated colorization are neural generative approaches based on log-likelihood estimation (Guadarrama et al., 2017; Royer et al., 2017; Ardizzone et al., 2019). Probabilistic models are a natural fit for the one-to-many task of image colorization and obtain better results than earlier determinisitic approaches avoiding some of the persistent pitfalls (Zhang et al., 2016). Probabilistic models also have the central advantage of producing multiple diverse colorings that are sampled from the learnt distribution.

In this paper, we introduce the Colorization Transformer (ColTran), a probabilistic colorization model composed only of axial self-attention blocks (Ho et al., 2019b; Wang et al., 2020). The main advantages of axial self-attention blocks are the ability to capture a global receptive field with only two layers and $\mathcal{O}(D\sqrt{D})$ instead of $\mathcal{O}(D^2)$ complexity. They can be implemented efficiently using

matrix-multiplications on modern accelerators such as TPUs (Jouppi et al., 2017). In order to enable colorization of high-resolution grayscale images, we decompose the task into three simpler sequential subtasks: coarse low resolution autoregressive colorization, parallel color and spatial upsampling. For coarse low resolution colorization, we apply a conditional variant of Axial Transformer (Ho et al., 2019b), a state-of-the-art autoregressive image generation model that does not require custom kernels (Child et al., 2019). While Axial Transformers support conditioning by biasing the input, we find that directly conditioning the transformer layers can improve results significantly. Finally, by leveraging the semi-parallel sampling mechanism of Axial Transformers we are able to colorize images faster at higher resolution than previous work (Guadarrama et al., 2017). This leads to improvements in colorization fidelity. Finally, we employ fast parallel deterministic upsampling models to super-resolve the coarsely colorized image into the final high resolution output. In summary, our main contributions are:

- First application of transformers for high-resolution (256×256) image colorization.
- We introduce conditional transformer layers for low-resolution coarse colorization in Section 4.1. The conditional layers incorporate conditioning information via multiple learnable components that are applied per-pixel and per-channel. We validate the contribution of each component with extensive experimentation and ablation studies.
- We propose training an auxiliary parallel prediction model jointly with the low resolution coarse colorization model in Section 4.2. Improved FID scores demonstrate the usefulness of this auxiliary model.
- We establish a new state-of-the-art on image colorization outperforming prior methods by a large margin on FID scores and a 2-Alternative Forced Choice (2AFC) Mechanical Turk test. Remarkably, in more than 60% of cases human evaluators prefer the highest rated among three generated colorings over the ground truth.

2 Related work

Colorization methods have initially relied on human-in-the-loop approaches to provide hints in the form of scribbles (Levin et al., 2004; Ironi et al., 2005; Huang et al., 2005; Yatziv & Sapiro, 2006; Qu et al., 2006; Luan et al., 2007; Tsaftaris et al., 2014; Zhang et al., 2017; Ci et al., 2018) and exemplar-based techniques that involve identifying a reference source image to copy colors from (Reinhard et al., 2001; Welsh et al., 2002; Tai et al., 2005; Ironi et al., 2005; Pitié et al., 2007; Morimoto et al., 2009; Gupta et al., 2012; Xiao et al., 2020). Exemplar based techniques have been recently extended to video as well (Zhang et al., 2019a). In the past few years, the focus has moved on to more automated, neural colorization methods. The deterministic colorization techniques such as CIC (Zhang et al., 2016), LRAC (Larsson et al., 2016), LTBC (Iizuka et al., 2016), Pix2Pix (Isola et al., 2017) and DC (Cheng et al., 2015; Dahl, 2016) involve variations of CNNs to model per-pixel color information conditioned on the intensity.

Generative colorization models typically extend unconditional image generation models to incorporate conditioning information from a grayscale image. Specifically, cINN (Ardizzone et al., 2019) use conditional normalizing flows (Dinh et al., 2014), VAE-MDN (Deshpande et al., 2017; 2015) and SCC-DC (Messaoud et al., 2018) use conditional VAEs (Kingma & Welling, 2013), and cGAN (Cao et al., 2017) use GANs (Goodfellow et al., 2014) for generative colorization. Most closely related to ColTran are other autoregressive approaches such as PixColor (Guadarrama et al., 2017) and PIC (Royer et al., 2017) with PixColor obtaining slightly better results than PIC due to its CNN-based upsampling strategy. ColTran is similar to PixColor in the usage of an autoregressive model for low resolution colorization and parallel spatial upsampling. ColTran differs from PixColor in the following ways. We train ColTran in a completely unsupervised fashion, while the conditioning network in PixColor requires pre-training with an object detection network that provides substantial semantic information. PixColor relies on PixelCNN (Oord et al., 2016) that requires a large depth to model interactions between all pixels. ColTran relies on Axial Transformer (Ho et al., 2019b) and can model all interactions between pixels with just 2 layers. PixColor uses different architectures for conditioning, colorization and super-resolution, while ColTran is conceptually simpler as we use self-attention blocks everywhere for both colorization and superresolution. Finally, we train our autoregressive model on a single coarse channel and a separate color upsampling network that improves fidelity (See: 5.3). The multi-stage generation process in ColTran that upsamples in depth

and in size is related to that used in Subscale Pixel Networks (Menick & Kalchbrenner, 2018) for image generation, with differences in the order and representation of bits as well as in the use of fully parallel networks. The self-attention blocks that are the building blocks of ColTran were initially developed for machine translation (Vaswani et al., 2017), but are now widely used in a number of other applications including density estimation (Parmar et al., 2018; Child et al., 2019; Ho et al., 2019a; Weissenborn et al., 2019) and GANs (Zhang et al., 2019b)

3 Background: Axial Transformer

3.1 Row and column self-attention

Self-attention (SA) has become a standard building block in many neural architectures. Although the complexity of self-attention is quadratic with the number of input elements (here pixels), it has become quite popular for image modeling recently (Parmar et al., 2018; Weissenborn et al., 2019) due to modeling innovations that don't require running global self-attention between all pixels. Following the work of (Ho et al., 2019b) we employ standard $\mathbf{qkv}$ self-attention (Vaswani et al., 2017) within rows and columns of an image. By alternating row- and column self-attention we effectively allow global exchange of information between all pixel positions. For the sake of brevity we omit the exact equations for multihead self-attention and refer the interested reader to the Appendix B for more details. Row/column attention layers are the core components of our model. We use them in the autoregressive colorizer, the spatial upsampler and the color upsampler.

3.2 Axial Transformer

Ths Axial Transformer (Ho et al., 2019b) is an autoregressive model that applies (masked) row- and column self-attention operations in a way that efficiently summarizes all past information $\mathbf{x}_{i,<j}$ and $\mathbf{x}_{<i,\cdot}$ to predict the next pixel at position i, j. Causal masking is employed by setting all $A_{m,n} = 0$ where $n > m$ during self-attention (see Eq. 15). The inputs to the model are the embedded pixels plus their respective position embeddings.

Outer decoder. The outer decoder computes a state $\mathbf{s}_o$ over all previous rows $\mathbf{x}_{\leq i,\cdot}$ by applying multiple layers of full row self-attention followed by masked column self-attention. (Eq 2). $\mathbf{s}_o$ is shifted down by a single row, such that the output representation $\mathbf{o}_{i,j}$ at position i, j only contains information about pixels $\mathbf{x}_{<i,\cdot}$ from prior rows. (Eq 3)

$$\mathbf{e} = \text{Embeddings}(\mathbf{x}) \tag{1}$$

$$\mathbf{s}_o = \text{MaskedColumn}(\text{Row}(\mathbf{e})) \qquad \times N \tag{2}$$

$$\mathbf{o} = \text{ShiftDown}(\mathbf{s}_o) \tag{3}$$

Inner decoder. The embeddings to the inner decoder are shifted right by a single column to mask the current pixel $\mathbf{x}_{i,j}$. The inner decoder adds the output of the outer decoder $\mathbf{o}$ to the shifted embeddings. It then computes a final state $\mathbf{h}$, by applying multiple layers of masked row-wise self-attention to infuse additional information from prior pixels of the same row $\mathbf{x}_{i,<j}$ (Eq 4). $\mathbf{h}_{i,j}$ comprises information about all past pixels $\mathbf{x}_{<i}$ and $\mathbf{x}_{i,<j}$. A dense layer projects $\mathbf{h}$ into a distribution $p(\mathbf{x}_{ij})$ over the pixel at position (i, j) conditioned on all previous pixels $\mathbf{x}_{i,<j}$ and $\mathbf{x}_{<i,\cdot}$.

$$\mathbf{z} = \mathbf{o} + \text{ShiftRight}(\mathbf{e}) \tag{4}$$

$$\mathbf{h} = \text{MaskedRow}(\mathbf{z}) \qquad \times N \tag{5}$$

$$p(\mathbf{x}_{ij}) = \text{Dense}(\mathbf{h}) \tag{6}$$

Encoder. As shown above, the outer and inner decoder operate on 2-D inputs, such as a single channel of an image. When modeling the "current channel", the Axial Transformer incorporates information from prior channels of an image (as per raster order) with an encoder. The encoder encodes each prior channel independently with a stack of unmasked row/column attention layers. The encoder outputs across all prior channels are summed to output a context representation $\mathbf{c}$ for the "current channel". The context representation conditions the outer and inner decoder by biasing the inputs in Eq 1 and Eq 4 respectively.

Component	Unconditional	Conditional
Self-Attention	$\mathbf{y} = \text{Softmax}(\frac{\mathbf{q}\mathbf{k}^\top}{\sqrt{D}})\mathbf{v}$	$\mathbf{y} = \text{Softmax}(\frac{\mathbf{q}_c\mathbf{k}_c^\top}{\sqrt{D}})\mathbf{v}_c$ where $\forall \mathbf{z} = \mathbf{k}, \mathbf{q}, \mathbf{v}$ $\mathbf{z}_c = (\mathbf{c}U_s^z) \odot \mathbf{z} + (\mathbf{c}U_b^z)$
MLP	$\mathbf{y} = \text{ReLU}(\mathbf{x}U_1 + \mathbf{b}_1)U_2 + \mathbf{b}_2$	$\mathbf{h} = \text{ReLU}(\mathbf{x}U_1 + \mathbf{b}_1)U_2 + \mathbf{b}_2$ $\mathbf{y} = (\mathbf{c}U_s^f) \odot \mathbf{h} + (\mathbf{c}U_b^f)$
Layer Norm	$\mathbf{y} = \beta\,\text{Norm}(\mathbf{x}) + \gamma$	$\mathbf{y} = \beta_c\,\text{Norm}(\mathbf{x}) + \gamma_c$ where $\forall \mu = \beta_c, \gamma_c$ $\mathbf{c} \in \mathbb{R}^{H\times W\times D} \rightarrow \hat{\mathbf{c}} \in \mathbb{R}^{HW\times D}$ $\mu = (\mathbf{u}\cdot\hat{\mathbf{c}})U_d^\mu \quad \mathbf{u} \in \mathbb{R}^{HW}$

Table 1: We contrast the different components of unconditional self-attention with self-attention conditioned on context $\mathbf{c} \in \mathbb{R}^{M\times N\times D}$. Learnable parameters specific to conditioning are denoted by $\mathbf{u}$ and $U_\cdot \in \mathbb{R}^{D\times D}$.

Sampling. The Axial Transformer natively supports semi-parallel sampling that avoids re-evaluation of the entire network to generate each pixel. The encoder is run once per-channel, the outer decoder is run once per row to predict context for all pixels for that particular row in parallel and only the inner decoder is run for every pixel.

4 Proposed Architecture

Image colorization is the task of transforming a grayscale image $x^g \in \mathbb{R}^{H\times W\times 1}$ into a colored image $x \in \mathbb{R}^{H\times W\times 3}$. The task is inherently stochastic; for a given grayscale image x^g, there exists a conditional distribution over x, $p(x|x^g)$. Instead of predicting x directly from x^g, we instead sequentially predict two intermediate low resolution images $x^{s\downarrow}$ and $x^{s\downarrow c\downarrow}$ with different color depth first. Besides simplifying the task of high-resolution image colorization into simpler tasks, the smaller resolution allows for training larger models.

We obtain $x^{s\downarrow}$, a spatially downsampled representation of x, by standard area interpolation. $x^{s\downarrow c\downarrow}$ is a 3 bit per-channel representation of $x^{s\downarrow}$, that is, each color channel has only 8 intensities. Thus, there are $8^3 = 512$ coarse colors per pixel which are predicted directly as a single "color" channel. We rewrite the conditional likelihood $p(x|x^g)$ to incorporate the intermediate representations as follows:

$$p(x|x^g) = p(x|x^g)\cdot 1 = p(x|x^g)\cdot p(x^{s\downarrow c\downarrow}, x^{s\downarrow}|x, x^g) = p(x^{s\downarrow c\downarrow}, x^{s\downarrow}, x|x^g) \tag{7}$$

$$= p(x|x^{s\downarrow}, x^g)\cdot p(x^{s\downarrow}|x^{s\downarrow c\downarrow}, x^g)\cdot p(x^{s\downarrow c\downarrow}|x^g) \tag{8}$$

ColTran core (Section 4.1), a parallel color upsampler and a parallel spatial upsampler (Section 4.3) model $p(x^{s\downarrow c\downarrow}|x^g), p(x^{s\downarrow}|x^{s\downarrow c\downarrow}, x^g)$ and $p(x|x^{s\downarrow})$ respectively. In the subsections below, we describe these individual components in detail. From now on we will refer to all low resolutions as $M \times N$ and high resolution as $H \times W$. An illustration of the overall architecture is shown in Figure 2.

4.1 ColTran Core

In this section, we describe ColTran core, a conditional variant of the Axial Transformer (Ho et al., 2019b) for low resolution coarse colorization. ColTran Core models a distribution $p_c(x^{s\downarrow c\downarrow}|x^g)$ over 512 coarse colors for every pixel, conditioned on a low resolution grayscale image in addition to the colors from previously predicted pixels as per raster order (Eq. 9).

$$p_c(x^{s\downarrow c\downarrow}|x^g) = \prod_{i=1}^{M}\prod_{j=1}^{N} p_c(x_{ij}^{s\downarrow c\downarrow}|x^g, x_{<i}^{s\downarrow c\downarrow}, x_{i,<j}^{s\downarrow c\downarrow}) \tag{9}$$

Given a context representation $\mathbf{c} \in \mathbb{R}^{M\times N\times D}$ we propose conditional transformer layers in Table 1. Conditional transformer layers have conditional versions of all components within the standard attention block (see Appendix B, Eqs. 14-18).

Conditional Self-Attention. For every layer in the decoder, we apply six 1×1 convolutions to $\mathbf{c}$ to obtain three scale and shift vectors which we apply element-wise to $\mathbf{q}$, $\mathbf{k}$ and $\mathbf{v}$ of the self-attention operation (Appendix 3.1), respectively.

Conditional MLP. A standard component of the transformer architecture is a two layer pointwise feed-forward network after the self-attention layer. We scale and shift to the output of each MLP conditioned on $\mathbf{c}$ as for self-attention.

Conditional Layer Norm. Layer normalization (Ba et al., 2016) globally scales and shifts a given normalized input using learnable vectors β, γ. Instead, we predict β_c and γ_c as a function of $\mathbf{c}$. We first aggregate $\mathbf{c}$ into a global 1-D representation $\overline{\mathbf{c}} \in \mathbb{R}^L$ via a learnable, spatial pooling layer. Spatial pooling is initialized as a mean pooling layer. Similar to 1-D conditional normalization layers (Perez et al., 2017; De Vries et al., 2017; Dumoulin et al., 2016; Huang & Belongie, 2017), we then apply a linear projection on $\overline{\mathbf{c}}$ to predict β_c and γ_c, respectively.

A grayscale encoder consisting of multiple, alternating row and column self-attention layers encodes the grayscale image into the initial conditioning context $\mathbf{c}^g$. It serves as both context for the conditional layers and as additional input to the embeddings of the outer decoder. The sum of the outer decoder's output and $\mathbf{c}^g$ condition the inner decoder. Figure 2 illustrates how conditioning is applied in the autoregressive core of the ColTran architecture.

Conditioning every layer via multiple components allows stronger gradient signals through the encoder and as an effect the encoder can learn better contextual representations. We validate this empirically by outperforming the native Axial Transformer that conditions context states by biasing (See Section 5.2 and Section 5.4).

4.2 Auxiliary parallel model

We additionally found it beneficial to train an auxiliary parallel prediction model that models $\widetilde{p}_c(x^{s\downarrow c\downarrow})$ directly on top of representations learned by the grayscale encoder which we found beneficial for regularization (Eq. 10)

$$\widetilde{p}_c(x^{s\downarrow c\downarrow}|x^g) = \prod_{i=1}^{M}\prod_{j=1}^{N} \widetilde{p}_c(x_{ij}^{s\downarrow c\downarrow}|x^g) \tag{10}$$

Intuitively, this forces the model to compute richer representations and global color structure already at the output of the encoder which can help conditioning and therefore has a beneficial, regularizing effect on learning. We apply a linear projection, $U_{\text{parallel}} \in \mathbb{R}^{L\times512}$ on top of $\mathbf{c}^g$ (the output of the grayscale encoder) into a per-pixel distribution over 512 coarse colors. It was crucial to tune the relative contribution of the autoregressive and parallel predictions to improve performance which we study in Section 5.3

4.3 Color & Spatial Upsampling

In order to produce high-fidelity colorized images from low resolution, coarse color images and a given high resolution grayscale image, we train color and spatial upsampling models. They share the same architecture while differing in their respective inputs and resolution at which they operate. Similar to the grayscale encoder, the upsamplers comprise of multiple alternating layers of row and column self-attention layers. The output of the encoder is projected to compute the logits underlying the per pixel color probabilities of the respective upsampler. Figure 2 illustrates the architectures

Color Upsampler. We convert the coarse image $x^{s\downarrow c\downarrow} \in \mathbb{R}^{M\times N\times1}$ of 512 colors back into a 3 bit RGB image with 8 symbols per channel. The channels are embedded using separate embedding matrices to $\mathbf{x}_k^{s\downarrow c\downarrow} \in \mathbb{R}^{M\times N\times D}$, where $k \in \{R, G, B\}$ indicates the channel. We upsample each channel individually conditioning only on the respective channel's embedding. The channel embedding is summed with the respective grayscale and position embedding for each pixel and serve as input to the subsequent self-attention layers (encoder). The output of the encoder is further projected to per pixel-channel probability distributions $\widetilde{p}_{c\uparrow}(x_k^{s\downarrow}|x^{s\downarrow c\downarrow}, x^g) \in \mathbb{R}^{M\times N\times256}$ over 256 color intensities

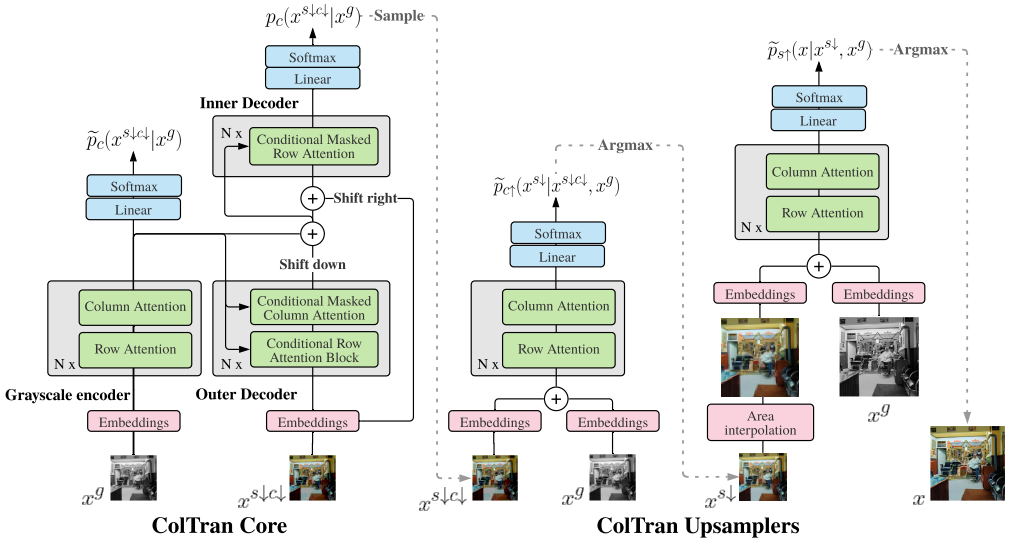

Figure 2: Depiction of ColTran. It consists of 3 individual models: an autoregressive colorizer (left), a color upsampler (middle) and a spatial upsampler (right). Each model is optimized independently. The autoregressive colorizer (ColTran core) is an instantiation of Axial Transformer (Sec. 3.2, Ho et al. (2019b)) with conditional transformer layers and an auxiliary parallel head proposed in this work (Sec. 4.1). During training, the ground-truth coarse low resolution image is both the input to the decoder and the target. Masked layers ensure that the conditional distributions for each pixel depends solely on previous ground-truth pixels. (See Appendix A for a recap on autoregressive models). ColTran upsamplers are stacked row/column attention layers that deterministically upsample color and space in parallel. Each attention block (in green) is residual and consists of the following operations: layer-norm $\rightarrow$ multihead self-attention $\rightarrow$ MLP.

for all $k \in \{R, G, B\}$ (Eq. 11).

$$\widetilde{p}_{c\uparrow}(x^{s\downarrow}|x^g) = \prod_{i=1}^{M}\prod_{j=1}^{N} \widetilde{p}_{c\uparrow}(x^{s\downarrow}_{ij}|x^g, x^{s\downarrow c\downarrow}) \tag{11}$$

Spatial Upsampler. We first naively upsample $x^{s\downarrow} \in \mathbb{R}^{M\times N\times 3}$ into a blurry, high-resolution RGB image using area interpolation. As above, we then embed each channel of the blurry RGB image and run a per-channel encoder exactly the same way as with the color upsampler. The output of the encoder is finally projected to per pixel-channel probability distributions $\widetilde{p}_{s\uparrow}(x_k|x^{s\downarrow}, x^g) \in \mathbb{R}^{H\times W\times 256}$ over 256 color intensities for all $k \in \{R, G, B\}$. (Eq. 12)

$$\widetilde{p}_{s\uparrow}(x|x^g) = \prod_{i=1}^{H}\prod_{j=1}^{W} \widetilde{p}_{s\uparrow}(x_{ij}|x^g, x^{s\downarrow}) \tag{12}$$

In our experiments, similar to (Guadarrama et al., 2017), we found parallel upsampling to be sufficient for high quality colorizations. Parallel upsampling has the huge advantage of fast generation which would be notoriously slow for full autoregressive models on high resolution. To avoid plausible minor color inconsistencies between pixels, instead of sampling each pixel from the predicted distribution in (Eq. 12 and Eq. 11), we just use the argmax. Even though this slightly limits the potential diversity of colorizations, in practice we observe that sampling only coarse colors via ColTran core is enough to produce a great variety of colorizations.

Objective. We train our architecture to minimize the negative log-likelihood (Eq. 13) of the data. $p_c/\widetilde{p}_c$, $\widetilde{p}_{s\uparrow}$, $\widetilde{p}_{c\uparrow}$ are maximized independently and λ is a hyperparameter that controls the relative contribution of p_c and $\widetilde{p}_c$

$$\mathcal{L} = (1-\lambda)\log p_c + \lambda \log \widetilde{p}_c + \log \widetilde{p}_{c\uparrow} + \log \widetilde{p}_{s\uparrow} \tag{13}$$

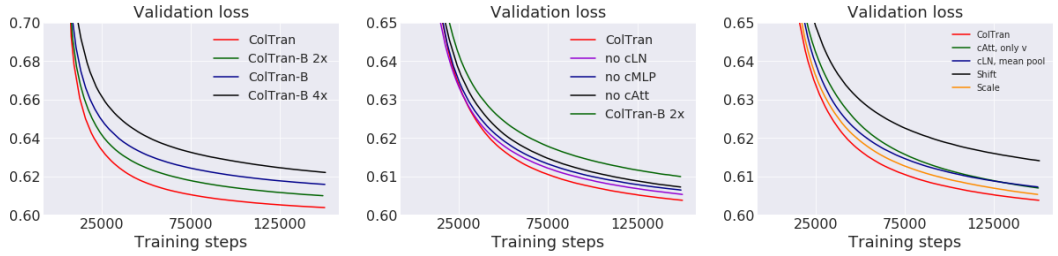

Figure 3: Per pixel log-likelihood of coarse colored 64×64 images over the validation set as a function of training steps. We ablate the various components of the ColTran core in each plot. **Left:** *ColTran* with Conditional Transformer Layers vs a baseline Axial Transformer which conditions via addition (*ColTran-B*). *ColTran-B 2x* and *ColTran-B 4x* refer to wider baselines with increased model capacity. **Center:** Removing each conditional sub-component one at a time (*no cLN*, *no cMLP* and *no cAtt*). **Right:** Conditional shifts only (*Shift*), Conditional scales only (*Scale*), removal of kq conditioning in cAtt (*cAtt, only v*) and fixed mean pooling in cLN (*cLN, mean pool*). See Section 5.2 for more details.

5 Experiments

5.1 Training and Evaluation

We evaluate ColTran on colorizing 256×256 grayscale images from the ImageNet dataset (Russakovsky et al., 2015). We train the ColTran core, color and spatial upsamplers independently on 16 TPUv2 chips with a batch-size of 224, 768 and 32 for 450K, 300K and 150K steps respectively. We use 4 axial attention blocks in each component of our architecture, with a hidden size of 512 and 4 heads. We use RMSprop (Tieleman & Hinton, 2012) with a fixed learning rate of $3e-4$. We set apart 10000 images from the training set as a holdout set to tune hyperparameters and perform ablations. To compute FID, we generate 5000 samples conditioned on the grayscale images from this holdout set. We use the public validation set to display qualitative results and report final numbers.

5.2 Ablations of ColTran Core

The autoregressive core of ColTran models downsampled, coarse-colored images of resolution 64×64 with 512 coarse colots, conditioned on the respective grayscale image. In a series of experiments we ablate the different components of the architecture (Figure 3). In the section below, we refer to the conditional self-attention, conditional layer norm and conditional MLP subcomponents as cAtt, cLN and cMLP respectively. We report the per-pixel log-likelihood over 512 coarse colors on the validation set as a function of training steps.

Impact of conditional transformer layers. The left side of Figure 3 illustrates the significant improvement in loss that ColTran core (with conditional transformer layers) achieves over the original Axial Transformer (marked *ColTran-B*). This demonstrates the usefulness of our proposed conditional layers. Because conditional layers introduce a higher number of parameters we additionally compare to and outperform the original Axial Transformer baselines with 2x and 4x wider MLP dimensions (labeled as *ColTran-B 2x* and *ColTran-B 4x*). Both *ColTran-B 2x* and *ColTran-B 4x* have an increased parameter count which makes for a fair comparison. Our results show that the increased performance cannot be explained solely by the fact that our model has more parameters.

Importance of each conditional component. We perform a leave-one-out study to determine the importance of each conditional component. We remove each conditional component one at a time and retrain the new ablated model. The curves *no cLN*, *no cMLP* and *no cAtt* in the middle of Figure 3 quantifies our results. While each conditional component improves final performance, cAtt plays the most important role.

Multiplicative vs Additive Interactions. Conditional transformer layers employ both conditional shifts and scales consisting of additive and multiplicative interactions, respectively. The curves *Scale* and *Shift* on the right hand side of Figure 3 demonstrate the impact of these interactions via ablated architectures that use conditional shifts and conditional scales only. While both types of interactions are important, multiplicative interactions have a much stronger impact.

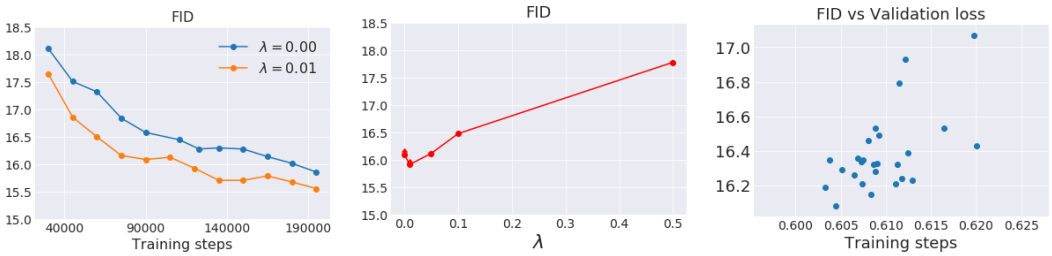

Figure 4: Left: FID of generated 64×64 coarse samples as a function of training steps for $\lambda = 0.01$ and $\lambda = 0.0$. **Center:** Final FID scores as a function of λ. **Right:** FID as a function of log-likelihood.

Context-aware dot product attention. Self-attention computes the similarity between pixel representations using a dot product between $\mathbf{q}$ and $\mathbf{k}$ (See: Eq 15). cAtt applies conditional shifts and scales on $\mathbf{q}$, $\mathbf{k}$ and allow modifying this similarity based on contextual information. The curve *cAtt, only v* on the right of Figure 3 shows that removing this property, by conditioning only on $\mathbf{v}$ leads to worse results.

Fixed vs adaptive global representation: cLN aggregates global information with a flexible learnable spatial pooling layer. We experimented with a fixed mean pooling layer forcing all the cLN layers to use the same global representation with the same per-pixel weight. The curve *cLN, mean pool* on the right of Figure 3 shows that enforcing this constraint causes inferior performance as compared to even having no cLN. This indicates that different aggregations of global representations are important for different cLN layers.

5.3 Other Ablations

Auxiliary Parallel Model. We study the effect of the hyperparameter λ, which controls the contribution of the auxiliary parallel prediction model described in Section 4.2. For a given λ, we now optimize $\hat{p}_c(\lambda) = (1 - \lambda) \log p_c(.) + \lambda \log \widetilde{p}_c(.)$ instead of just $\log p_c(.)$. Note that $\widetilde{p}_c(.)$, models each pixel independently, which is more difficult than modelling each pixel conditioned on previous pixels given by $p_c(.)$. Hence, employing $\hat{p}_c(\lambda)$ as a holdout metric, would just lead to a trivial soluion at $\lambda = 0$. Instead, the FID of the generated coarse 64x64 samples provides a reliable way to find an optimal value of λ. In Figure 4, at $\lambda = 0.01$, our model converges to a better FID faster with a marginal but consistent final improvement. At higher values the performance deteriorates quickly.

Upsamplers. Upsampling coarse colored, low-resolution images to a higher resolution is much simpler. Given ground truth 64×64 coarse images, the ColTran upsamplers map these to fine grained 256×256 images without any visible artifacts and FID of 16.4. For comparison, the FID between two random sets of 5000 samples from our holdout set is 15.5. It is further extremely important to provide the grayscale image as input to each of the individual upsamplers, without which the generated images appear highly smoothed out and the FID drops to 27.0. We also trained a single upsampler for both color and resolution. The FID in this case, drops marginally to 16.6.

5.4 Frechet Inception Distance

We compute FID using colorizations of 5000 grayscale images of resolution 256×256 from the ImageNet validation set as done in (Ardizzone et al., 2019). In addition to ColTran, we report two additional results *ColTran-S* and *ColTran-Baseline*. *ColTran-B* refers to the baseline Axial Transformer that conditions via addition at the input. PixColor samples smaller 28×28 colored images autoregressively as compared to ColTran's 64×64. As a control experiment, we train an autoregressive model on resolution 28×28 (*ColTran-S*) to disentangle architectural choices and the inherent stochasticity of modelling higher resolution images. *ColTran-S* and *ColTran-B* obtains FID scores of 21.9 and 21.6 that significantly improve over the previous best FID of 24.32. Finally, ColTran achieves the best FID score of 19.71. All results are presented in Table 2 left.

Correlation between FID and Log-likelihood. For each architectural variant, Figure 4 right illustrates the correlation between the log-likelihood and FID after 150K training steps. There is a

Models	FID
ColTran	**19.71 ± 0.12**
ColTran-B [19]	21.6 ± 0.13
ColTran-S	21.9 ± 0.09
PixColor [16]	24.32 ± 0.21
cGAN [3]	24.41 ± 0.27
cINN [1]	25.13 ± 0.3
VAE-MDN [11]	25.98 ± 0.28
Ground truth	14.68 ± 0.15
Grayscale	30.19 ± 0.1

Models	AMT Fooling rate
ColTran (Oracle)	62.0 % ± 0.99
ColTran (Seed 1)	40.5 % ± 0.81
ColTran (Seed 2)	**42.3 % ± 0.76**
ColTran (Seed 3)	41.7 % ± 0.83
PixColor [16] (Oracle)	38.3 % ± 0.98
PixColor (Seed 1)	33.3 % ± 1.04
PixColor (Seed 2)	35.4 % ± 1.01
PixColor (Seed 3)	33.2 % ± 1.03
CIC [56]	29.2 % ± 0.98
LRAC [27]	30.9 % ± 1.02
LTBC [22]	25.8 % ± 0.97

Table 2: We outperform various state-of-the-art colorization models both on FID (left) and human evaluation (right). We obtain the FID scores from (Ardizzone et al., 2019) and the human evaluation results from (Guadarrama et al., 2017). ColTran-B is a baseline Axial Transformer that conditions via addition and ColTran-S is a control experiment where we train ColTran core (See: 4.1) on smaller 28 × 28 colored images.

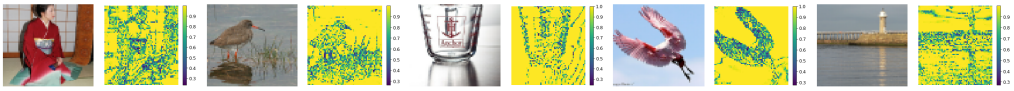

Figure 5: We display the per-pixel, maximum predicted probability over 512 colors as a proxy for uncertainty.

moderately positive correlation of 0.57 between the log-likelihood and FID. Importantly, even an absolute improvement on the order of 0.01 - 0.02 can improve FID significantly. This suggests that designing architectures that achieve better log-likelihood values is likely to lead to improved FID scores and colorization fidelity.

5.5 Qualitative Evaluation

Human Evaluation. For our qualitative assessment, we follow the protocol used in PixColor (Guadarrama et al., 2017). ColTran colorizes 500 grayscale images, with 3 different colorizations per image, denoted as seeds. Human raters assess the quality of these colorizations with a two alternative-forced choice (2AFC) test. We display both the ground-truth and recolorized image sequentially for one second in random order. The raters are then asked to identify the image with fake colors. For each seed, we report the mean fooling rate over 500 colorizations and 5 different raters. For the oracle methods, we use the human rating to pick the best-of-three colorizations. ColTran's best seed achieves a fooling rate of 42.3 % compared to the 35.4 % of PixColor's best seed. ColTran Oracle achieves a fooling rate of 62 %, indicating that human raters prefer ColTran's best-of-three colorizations over the ground truth image itself.

Visualizing uncertainty. The autoregressive core model of ColTran should be highly uncertain at object boundaries when colors change. Figure 12 illustrates the per-pixel, maximum predicted probability over 512 colors as a proxy for uncertainty. We observe that the model is indeed highly uncertain at edges and within more complicated textures.

6 Conclusions

We presented the Colorization Transformer (ColTran), an architecture that entirely relies on self-attention for image colorization. We introduce a conditional self-attention, a novel building block for conditional, generative models based on self-attention. Our ablations show the superiority of employing this mechanism over a number of different baselines. ColTran achieves very strong empirical results, outperforming prior state-of-the-art by a large margin. Finally, we demonstrate that ColTran can generate diverse, high-fidelity colorizations on ImageNet, which are largely indistinguishable from the ground-truth even for human raters.

REFERENCES

Lynton Ardizzone, Carsten Lüth, Jakob Kruse, Carsten Rother, and Ullrich Köthe. Guided image generation with conditional invertible neural networks. *arXiv preprint arXiv:1907.02392*, 2019.

Jimmy Lei Ba, Jamie Ryan Kiros, and Geoffrey E Hinton. Layer normalization. *arXiv preprint arXiv:1607.06450*, 2016.

Yun Cao, Zhiming Zhou, Weinan Zhang, and Yong Yu. Unsupervised diverse colorization via generative adversarial networks, 2017.

Zezhou Cheng, Qingxiong Yang, and Bin Sheng. Deep colorization. In *Proceedings of the IEEE International Conference on Computer Vision*, pp. 415–423, 2015.

Rewon Child, Scott Gray, Alec Radford, and Ilya Sutskever. Generating long sequences with sparse transformers. *arXiv preprint arXiv:1904.10509*, 2019.

Yuanzheng Ci, Xinzhu Ma, Zhihui Wang, Haojie Li, and Zhongxuan Luo. User-guided deep anime line art colorization with conditional adversarial networks. In *Proceedings of the 26th ACM international conference on Multimedia*, pp. 1536–1544, 2018.

Ceyda Cinarel and Byoung-Tak Zhang. Into the colorful world of webtoons: Through the lens of neural networks. In *2017 14th IAPR International Conference on Document Analysis and Recognition (ICDAR)*, volume 3, pp. 35–40. IEEE, 2017.

Ryan Dahl. Automatic colorization, 2016.

Harm De Vries, Florian Strub, Jérémie Mary, Hugo Larochelle, Olivier Pietquin, and Aaron C Courville. Modulating early visual processing by language. In *Advances in Neural Information Processing Systems*, pp. 6594–6604, 2017.

Aditya Deshpande, Jason Rock, and David Forsyth. Learning large-scale automatic image colorization. In *Proceedings of the IEEE International Conference on Computer Vision*, pp. 567–575, 2015.

Aditya Deshpande, Jiajun Lu, Mao-Chuang Yeh, Min Jin Chong, and David Forsyth. Learning diverse image colorization. In *Proceedings of the IEEE Conference on Computer Vision and Pattern Recognition*, pp. 6837–6845, 2017.

Laurent Dinh, David Krueger, and Yoshua Bengio. Nice: Non-linear independent components estimation. *arXiv preprint arXiv:1410.8516*, 2014.

Vincent Dumoulin, Jonathon Shlens, and Manjunath Kudlur. A learned representation for artistic style. *arXiv preprint arXiv:1610.07629*, 2016.

David M Geshwind. Method for colorizing black and white footage, August 19 1986. US Patent 4,606,625.

Ian J Goodfellow, Jean Pouget-Abadie, Mehdi Mirza, Bing Xu, David Warde-Farley, Sherjil Ozair, Aaron Courville, and Yoshua Bengio. Generative adversarial networks. *arXiv preprint arXiv:1406.2661*, 2014.

Sergio Guadarrama, Ryan Dahl, David Bieber, Mohammad Norouzi, Jonathon Shlens, and Kevin Murphy. Pixcolor: Pixel recursive colorization. *arXiv preprint arXiv:1705.07208*, 2017.

Raj Kumar Gupta, Alex Yong-Sang Chia, Deepu Rajan, Ee Sin Ng, and Huang Zhiyong. Image colorization using similar images. In *Proceedings of the 20th ACM international conference on Multimedia*, pp. 369–378, 2012.

Jonathan Ho, Xi Chen, Aravind Srinivas, Yan Duan, and Pieter Abbeel. Flow++: Improving flow-based generative models with variational dequantization and architecture design. *arXiv preprint arXiv:1902.00275*, 2019a.

Jonathan Ho, Nal Kalchbrenner, Dirk Weissenborn, and Tim Salimans. Axial attention in multidimensional transformers. *arXiv preprint arXiv:1912.12180*, 2019b.

Xun Huang and Serge Belongie. Arbitrary style transfer in real-time with adaptive instance normalization. In *Proceedings of the IEEE International Conference on Computer Vision*, pp. 1501–1510, 2017.

Yi-Chin Huang, Yi-Shin Tung, Jun-Cheng Chen, Sung-Wen Wang, and Ja-Ling Wu. An adaptive edge detection based colorization algorithm and its applications. In *Proceedings of the 13th annual ACM international conference on Multimedia*, pp. 351–354, 2005.

Satoshi Iizuka, Edgar Simo-Serra, and Hiroshi Ishikawa. Let there be color! joint end-to-end learning of global and local image priors for automatic image colorization with simultaneous classification. *ACM Transactions on Graphics (ToG)*, 35(4):1–11, 2016.

Revital Ironi, Daniel Cohen-Or, and Dani Lischinski. Colorization by example. In *Rendering Techniques*, pp. 201–210. Citeseer, 2005.

Phillip Isola, Jun-Yan Zhu, Tinghui Zhou, and Alexei A Efros. Image-to-image translation with conditional adversarial networks. In *Proceedings of the IEEE conference on computer vision and pattern recognition*, pp. 1125–1134, 2017.

Norman P. Jouppi, Cliff Young, Nishant Patil, David Patterson, Gaurav Agrawal, Raminder Bajwa, Sarah Bates, Suresh Bhatia, Nan Boden, Al Borchers, Rick Boyle, Pierre luc Cantin, Clifford Chao, Chris Clark, Jeremy Coriell, Mike Daley, Matt Dau, Jeffrey Dean, Ben Gelb, Tara Vazir Ghaemmaghami, Rajendra Gottipati, William Gulland, Robert Hagmann, C. Richard Ho, Doug Hogberg, John Hu, Robert Hundt, Dan Hurt, Julian Ibarz, Aaron Jaffey, Alek Jaworski, Alexander Kaplan, Harshit Khaitan, Andy Koch, Naveen Kumar, Steve Lacy, James Laudon, James Law, Diemthu Le, Chris Leary, Zhuyuan Liu, Kyle Lucke, Alan Lundin, Gordon MacKean, Adriana Maggiore, Maire Mahony, Kieran Miller, Rahul Nagarajan, Ravi Narayanaswami, Ray Ni, Kathy Nix, Thomas Norrie, Mark Omernick, Narayana Penukonda, Andy Phelps, Jonathan Ross, Matt Ross, Amir Salek, Emad Samadiani, Chris Severn, Gregory Sizikov, Matthew Snelham, Jed Souter, Dan Steinberg, Andy Swing, Mercedes Tan, Gregory Thorson, Bo Tian, Horia Toma, Erick Tuttle, Vijay Vasudevan, Richard Walter, Walter Wang, Eric Wilcox, and Doe Hyun Yoon. In-datacenter performance analysis of a tensor processing unit, 2017.

Diederik P Kingma and Max Welling. Auto-encoding variational bayes. *arXiv preprint arXiv:1312.6114*, 2013.

Gustav Larsson, Michael Maire, and Gregory Shakhnarovich. Learning representations for automatic colorization. In *European conference on computer vision*, pp. 577–593. Springer, 2016.

Anat Levin, Dani Lischinski, and Yair Weiss. Colorization using optimization. In *ACM SIGGRAPH 2004 Papers*, pp. 689–694. 2004.

Ziwei Liu, Ping Luo, Xiaogang Wang, and Xiaoou Tang. Deep learning face attributes in the wild. In *Proceedings of the IEEE international conference on computer vision*, pp. 3730–3738, 2015.

Qing Luan, Fang Wen, Daniel Cohen-Or, Lin Liang, Ying-Qing Xu, and Heung-Yeung Shum. Natural image colorization. In *Proceedings of the 18th Eurographics conference on Rendering Techniques*, pp. 309–320, 2007.

Jacob Menick and Nal Kalchbrenner. Generating high fidelity images with subscale pixel networks and multidimensional upscaling. *arXiv preprint arXiv:1812.01608*, 2018.

Safa Messaoud, David Forsyth, and Alexander G. Schwing. Structural consistency and controllability for diverse colorization. In *Proceedings of the European Conference on Computer Vision (ECCV)*, September 2018.

Yuji Morimoto, Yuichi Taguchi, and Takeshi Naemura. Automatic colorization of grayscale images using multiple images on the web. In *SIGGRAPH 2009: Talks*, pp. 1–1. 2009.

Aaron van den Oord, Nal Kalchbrenner, and Koray Kavukcuoglu. Pixel recurrent neural networks. *arXiv preprint arXiv:1601.06759*, 2016.

Niki Parmar, Ashish Vaswani, Jakob Uszkoreit, Łukasz Kaiser, Noam Shazeer, Alexander Ku, and Dustin Tran. Image transformer. *arXiv preprint arXiv:1802.05751*, 2018.

Ethan Perez, Florian Strub, Harm De Vries, Vincent Dumoulin, and Aaron Courville. Film: Visual reasoning with a general conditioning layer. *arXiv preprint arXiv:1709.07871*, 2017.

François Pitié, Anil C Kokaram, and Rozenn Dahyot. Automated colour grading using colour distribution transfer. *Computer Vision and Image Understanding*, 107(1-2):123–137, 2007.

Yingge Qu, Tien-Tsin Wong, and Pheng-Ann Heng. Manga colorization. *ACM Transactions on Graphics (TOG)*, 25(3):1214–1220, 2006.

Erik Reinhard, Michael Adhikhmin, Bruce Gooch, and Peter Shirley. Color transfer between images. *IEEE Computer graphics and applications*, 21(5):34–41, 2001.

Amelie Royer, Alexander Kolesnikov, and Christoph H Lampert. Probabilistic image colorization. *arXiv preprint arXiv:1705.04258*, 2017.

Olga Russakovsky, Jia Deng, Hao Su, Jonathan Krause, Sanjeev Satheesh, Sean Ma, Zhiheng Huang, Andrej Karpathy, Aditya Khosla, Michael Bernstein, et al. Imagenet large scale visual recognition challenge. *International journal of computer vision*, 115(3):211–252, 2015.

Daniel Sỳkora, Jan Buriánek, and Jiří Žára. Unsupervised colorization of black-and-white cartoons. In *Proceedings of the 3rd international symposium on Non-photorealistic animation and rendering*, pp. 121–127, 2004.

Yu-Wing Tai, Jiaya Jia, and Chi-Keung Tang. Local color transfer via probabilistic segmentation by expectation-maximization. In *2005 IEEE Computer Society Conference on Computer Vision and Pattern Recognition (CVPR'05)*, volume 1, pp. 747–754. IEEE, 2005.

Tijmen Tieleman and Geoffrey Hinton. Lecture 6.5-rmsprop: Divide the gradient by a running average of its recent magnitude. *COURSERA: Neural networks for machine learning*, 4(2):26–31, 2012.

Sotirios A Tsaftaris, Francesca Casadio, Jean-Louis Andral, and Aggelos K Katsaggelos. A novel visualization tool for art history and conservation: Automated colorization of black and white archival photographs of works of art. *Studies in conservation*, 59(3):125–135, 2014.

Ashish Vaswani, Noam Shazeer, Niki Parmar, Jakob Uszkoreit, Llion Jones, Aidan N Gomez, Łukasz Kaiser, and Illia Polosukhin. Attention is all you need. In *Advances in neural information processing systems*, pp. 5998–6008, 2017.

Carl Vondrick, Abhinav Shrivastava, Alireza Fathi, Sergio Guadarrama, and Kevin Murphy. Tracking emerges by colorizing videos. In *Proceedings of the European conference on computer vision (ECCV)*, pp. 391–408, 2018.

Huiyu Wang, Yukun Zhu, Bradley Green, Hartwig Adam, Alan Yuille, and Liang-Chieh Chen. Axial-deeplab: Stand-alone axial-attention for panoptic segmentation. *arXiv preprint arXiv:2003.07853*, 2020.

Dirk Weissenborn, Oscar Täckström, and Jakob Uszkoreit. Scaling autoregressive video models. *arXiv preprint arXiv:1906.02634*, 2019.

Tomihisa Welsh, Michael Ashikhmin, and Klaus Mueller. Transferring color to greyscale images. In *Proceedings of the 29th annual conference on Computer graphics and interactive techniques*, pp. 277–280, 2002.

Chufeng Xiao, Chu Han, Zhuming Zhang, Jing Qin, Tien-Tsin Wong, Guoqiang Han, and Shengfeng He. Example-based colourization via dense encoding pyramids. In *Computer Graphics Forum*, volume 39, pp. 20–33. Wiley Online Library, 2020.

Liron Yatziv and Guillermo Sapiro. Fast image and video colorization using chrominance blending. *IEEE transactions on image processing*, 15(5):1120–1129, 2006.

Fisher Yu, Ari Seff, Yinda Zhang, Shuran Song, Thomas Funkhouser, and Jianxiong Xiao. Lsun: Construction of a large-scale image dataset using deep learning with humans in the loop. *arXiv preprint arXiv:1506.03365*, 2015.

Bo Zhang, Mingming He, Jing Liao, Pedro V Sander, Lu Yuan, Amine Bermak, and Dong Chen. Deep exemplar-based video colorization. In *Proceedings of the IEEE Conference on Computer Vision and Pattern Recognition*, pp. 8052–8061, 2019a.

Han Zhang, Ian Goodfellow, Dimitris Metaxas, and Augustus Odena. Self-attention generative adversarial networks. In *International Conference on Machine Learning*, pp. 7354–7363. PMLR, 2019b.

Richard Zhang, Phillip Isola, and Alexei A Efros. Colorful image colorization. In *European conference on computer vision*, pp. 649–666. Springer, 2016.

Richard Zhang, Jun-Yan Zhu, Phillip Isola, Xinyang Geng, Angela S Lin, Tianhe Yu, and Alexei A Efros. Real-time user-guided image colorization with learned deep priors. *arXiv preprint arXiv:1705.02999*, 2017.

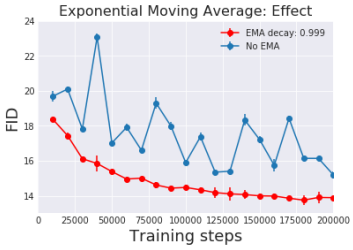

Figure 6: FID vs training steps, with and without polyak averaging.

A AUTOREGRESSIVE MODELS

Autoregressive models are a family of probabilistic methods that model joint distribution of data $P(x)$ or a sequence of symbols $(x_1, x_2, \dots x_n)$ as a product of conditionals $\prod_{i=1}^{N} P(x_i|x_{<i})$. During training, the input to autoregressive models are the entire sequence of ground-truth symbols. Masking ensures that the contribution of all "future" symbols in the sequence are zeroed out. The outputs of the autoregressive model are the corresponding conditional distributions. $P(x_i|x_{<i})$. Optimizing the parameters of the autoregressive model proceeds by a standard log-likelihood objective.

Generation happens sequentially, symbol-by-symbol. Once a symbol x_i is generated, the entire sequence $(x_1, x_2, \dots x_i)$ are fed to the autoregressive model to generate x_{i+1}.

In the case of autoregressive image generation symbols typically correspond to the 3 RGB pixel-channel. These are generated sequentially in raster-scan order, channel by channel and pixel by pixel.

B ROW/COLUMN SELF-ATTENTION

In the following we describe row self-attention, that is, we omit the height dimension as all operations are performed in parallel for each column. Given the representation of a single row within of an image $\mathbf{x}_{i,\cdot} \in \mathbb{R}^{W \times D}$, row-wise self-attention block is applied as follows:

$$[\mathbf{q}, \mathbf{k}, \mathbf{v}] = \mathrm{LN}(\mathbf{x}_{i,\cdot}) U_{qkv} \qquad U_{qkv} \in \mathbb{R}^{D \times 3D_h} \tag{14}$$

$$A = \mathrm{softmax}\left(\mathbf{q}\mathbf{k}^\top / \sqrt{D_h}\right) \qquad A \in \mathbb{R}^{W \times W} \tag{15}$$

$$\mathrm{SA}(\mathbf{x}_{i,\cdot}) = A\mathbf{v} \tag{16}$$

$$\mathrm{MSA}(\mathbf{x}_{i,\cdot}) = [\mathrm{SA}_1(\mathbf{x}_{i,\cdot}), \mathrm{SA}_2(\mathbf{x}_{i,\cdot}), \cdots, \mathrm{SA}_k(\mathbf{x}_{i,\cdot})]\, U_{out} \qquad U_{out} \in \mathbb{R}^{k \cdot D_h \times D} \tag{17}$$

LN refers to the application of layer normalization (Ba et al., 2016). Finally, we apply residual connections and a feed-forward neural network with a single hidden layer and ReLU activation (MLP) after each self-attention block as it is common practice in transformers.

$$\hat{\mathbf{x}}_{i,\cdot} = \mathrm{MLP}(\mathrm{LN}(\mathbf{x}'_{i,\cdot})) + \mathbf{x}'_{i,\cdot} \qquad \mathbf{x}'_{i,\cdot} = \mathrm{MSA}(\mathbf{x}_{i,\cdot}) + \mathbf{x}_{i,\cdot} \tag{18}$$

Column-wise self-attention over $\mathbf{x}_{\cdot,j} \in \mathbb{R}^{H \times D}$ works analogously.

C EXPONENTIAL MOVING AVERAGE

We found using an exponential moving average (EMA) of our checkpoints, extremely crucial to generate high quality samples. In Figure 6, we display the FID as a function of training steps, with and without EMA. On applying EMA, our FID score improves steadily over time.

D OUT OF DOMAIN COLORIZATIONS

We use our trained colorization model on ImageNet to colorize high-resolution grayscale images from LSUN 256×256 (Yu et al., 2015) and low-resolution grayscale images from Celeb-A (Liu

Figure 7: We train our colorization model on ImageNet and display high resolution colorizations from LSUN

Figure 8: We train our colorization model on ImageNet and display low resolution colorizations from Celeb-A

Figure 9: Ablated models. *Gated*: Gated conditioning layers as done in (Oord et al., 2016) and *cAtt + cMLP, global*: Global conditioning instead of pointwise conditioning in cAtt and cLN.

et al., 2015) 64×64. Note that these models were trained only on ImageNet and not finetuned on Celeb-A or LSUN.

E Low batch-size regime

We retrained the autoregressive colorizer and color upsampler on 4 TPUv2 chips (the lowest configuration) with a reduced-batch size of 56 and 192 each. For the spatial upsampler, we found that a batch-size of 8 was sub-optimal and lead to a large deterioration in loss. We thus used a smaller spatial upsampler with 2 axial attention blocks with a batch-size of 16 and trained it also on 4 TPUv2 chips. The FID drops from 19.71 to 20.9 which is still significantly better than the other models in 2. We note that in this experiment, we use only 12 TPUv2 chips in total while PixColor (Guadarrama et al., 2017) uses a total of 16 GPUs.

F Number of axial attention blocks

We did a very small hyperparameter sweep using the baseline axial transformer (no conditional layers) with the following configurations:

- hidden size = 512, number of blocks = 4
- hidden size = 1024, number of blocks = 2
- hidden size = 512, number of blocks = 2

Once we found the optimal configuration, we fixed this for all future architecture design.

G Additional ablations:

We perform additional ablations comparing conditional transformer layers based on Gated layers (Oord et al., 2016) (*Gated*) and a global conditioning layer instead of pointwise conditioning in cAtt and cLN. *cAtt + cMLP, global*.

H Number of parameters and inference speed

Inference speed. ColTran core can sample 64x64 grayscale images in 4-5 minutes P100 GPU vs PixColor that takes 10 minutes to colorize 28x28 grayscale images on a K40 GPU. Sampling 28x28 colorizations takes just around 30 seconds. The upsampler networks take in the order of milliseconds.

Number of parameters. ColTran has a total of ColTran core (46M) + Color Upsampler (14M) + Spatial Upsampler (14M) = 74M parameters. This is lesser than PixColor that has Conditioning network (44M) + Colorizer network (11M) + Refinement Network (28M) = 83M parameters.

Figure 10: Top: Colorizations **Bottom**: Ground truth. From left to right, our colorizations have a progressively higher fooling rate.

Figure 11: In each column, we display the ground truth followed by 3 samples. **Left:** Diverse and real. **Center:** Realism improves from left to right. **Right:** Failure cases

I ANALYSIS OF MTURK RATINGS

We analyzed our samples on the basis of the MTurk ratings in Figure 11. To the left, we show images, where all the samples have a fool rate > 60 %. Our model is able to show diversity in color for both high-level structure and low-level details. In the center, we display samples that have a high variance in MTurk ratings, with a difference of 80 % between the best and the worst sample. All of these are complex objects, that our model is able to colorize reasonably well given multiple attempts. To the right of Figure 11, we show failure cases where all samples have a fool rate of 0 %, For these cases, our model is unable to colorize highly complex structure, that would arguably be difficult even for a human.

J MORE PROBABILITY MAPS

We display additional probability maps to visualize uncertainty as done in 5.5.

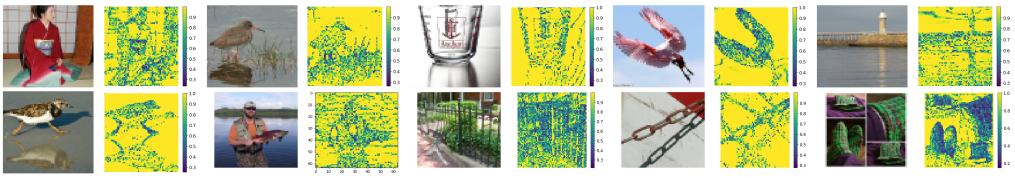

Figure 12: We display the per-pixel, maximum predicted probability over 512 colors as a proxy for uncertainty.

K MORE SAMPLES

We display a wide-diversity of colorizations from ColTran that were not cherry-picked.

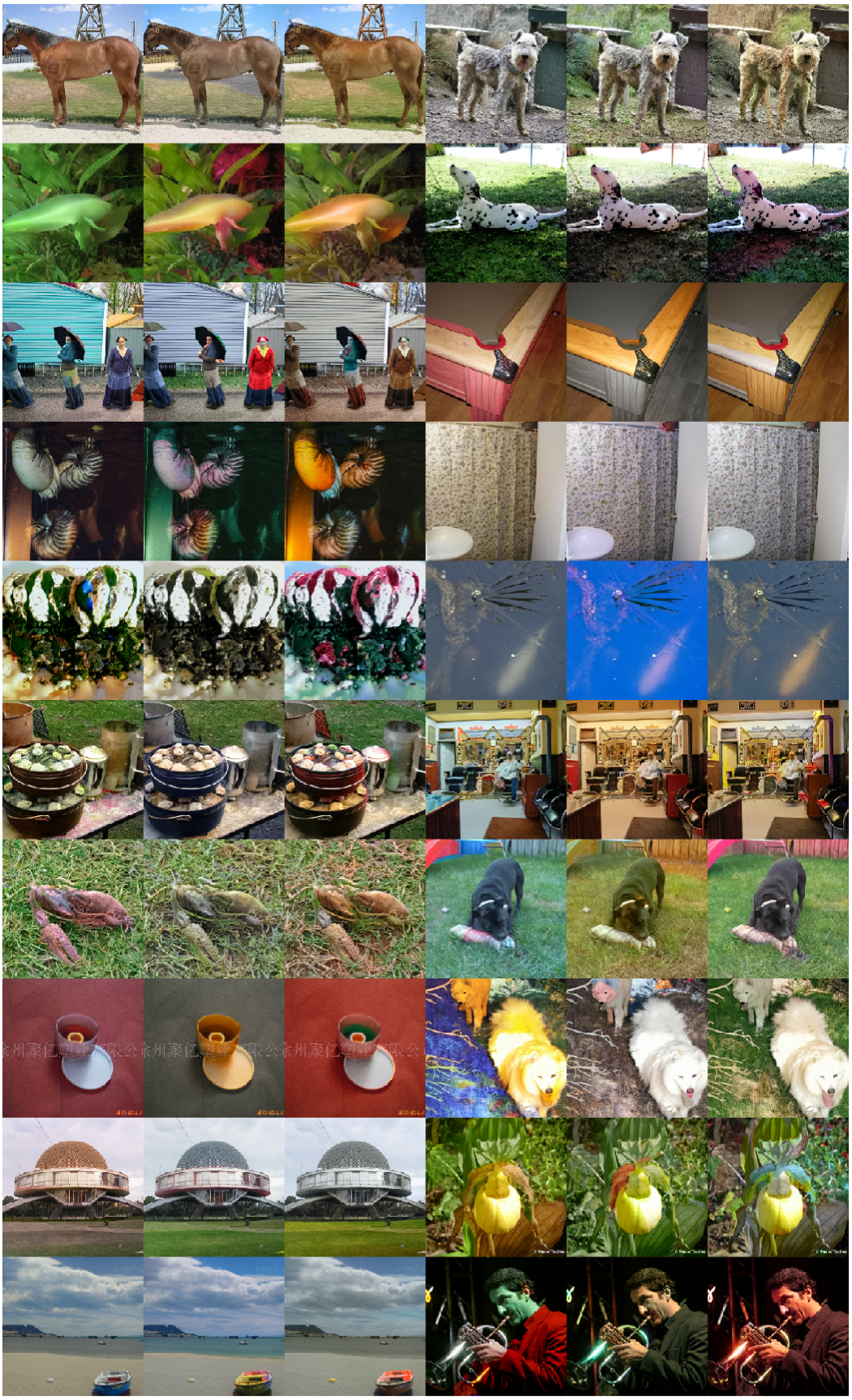

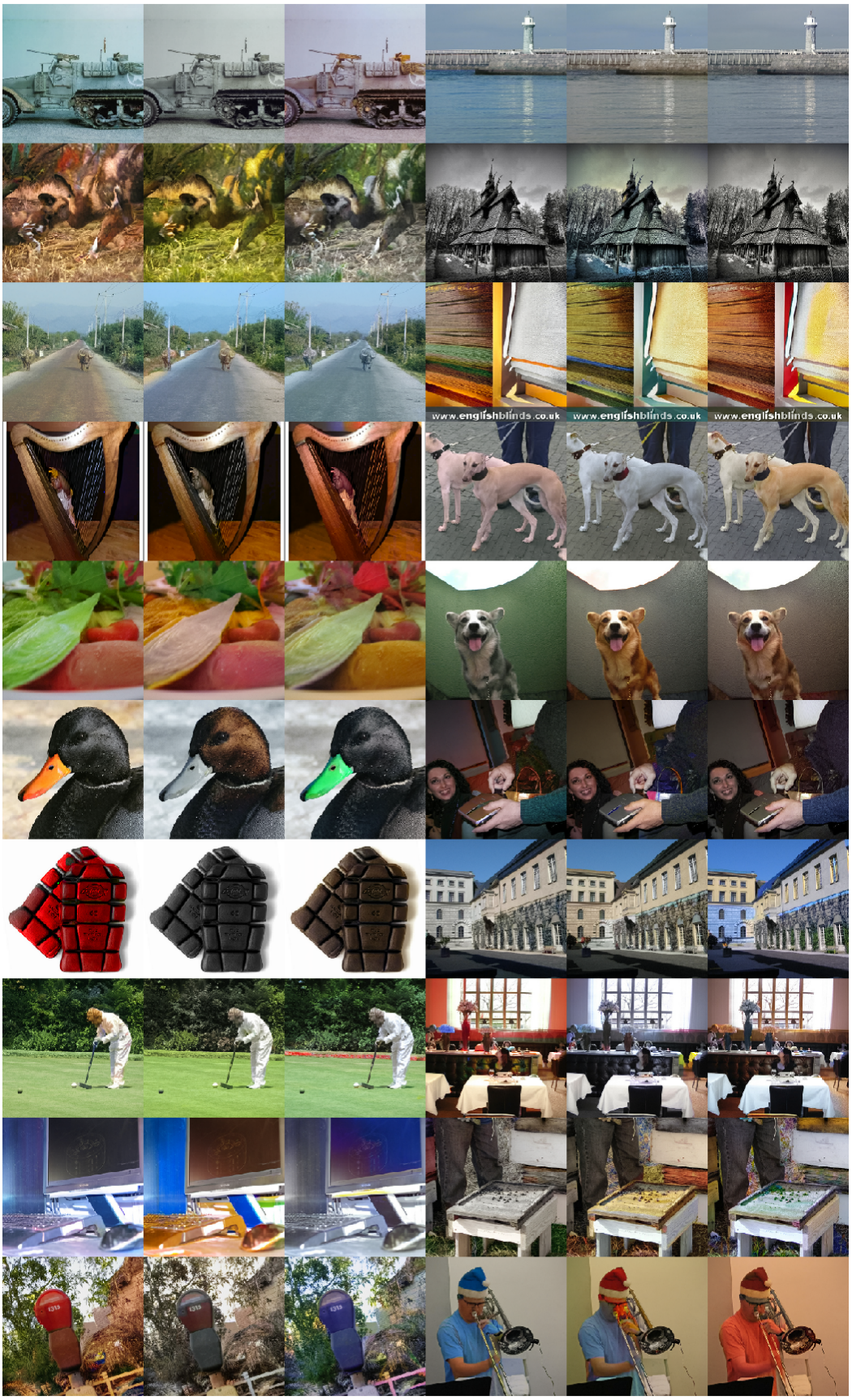
www.englishblinds.co.uk
www.englishblinds.co.uk
www.englishblinds.co.uk

iStockphoto
iStockphoto
iStockphoto
OXO
OXO
OXO
NERO
NERO
NERO
AURICS REMOVALS
AURICS REMOVALS
AURICS REMOVALS

NERO
AURICS REMOVALS